Contribution from the Department of Chemistry, University of Houston, Houston, Texas 77004, Faculté des Sciences de Rabat, Laboratoire de Chimie Physique Générale, Université Mohammed V, Rabat, Morocco, and Laboratoire de Synthèse et d'Electrosynthèse Organométallique. Associé au CNRS (UA 33), Faculté des Sciences "Gabriel", 21100 Dijon, France

Electrochemistry of Vanadyl Porphyrins in Dimethylformamide

K. M. Kadish,*[1a] D. Sazou,[1a] C. Araullo,[1a] Y. M. Liu,[1a] A. Saoiabi,[1b] M. Ferhat,[1b] and R. Guilard*[1c]

Received September 3, 1987

The electrochemistry of (P)VO in DMF is reported where P is the dianion of tetrapyridylporphyrin (TpyP), tetrakis(*p*-sulfonatophenyl)porphyrin (T(*p*-SO_3Na)PP), or tetrakis(*p*-(diethylamino)phenyl)porphyrin (T(*p*-Et_2N)PP). (TpyP)VO and (T(*p*-SO_3Na)PP)VO are able to bind a sixth axial ligand, and values of formation constants for DMF addition to $[(P)VO]^-$ and (P)VO in CH_2Cl_2 were calculated by using electrochemical and spectral methods. The [T(*p*-Et_2N)PP]VO complex does not axially bind DMF. Electrode reactions of the three vanadyl complexes were monitored in DMF by cyclic voltammetry, rotating-disk voltammetry, and spectroelectrochemistry. Each complex is reduced in two one-electron-transfer steps to give a π anion radical and a dianion. [T(*p*-SO_3Na)PP]VO and [T(*p*-Et_2N)PP]VO undergo several oxidations in DMF, but (TpyP)VO is not oxidized within the potential range of the solvent. The first one-electron abstraction from [T(*p*-SO_3Na)PP]VO and [T(*p*-Et_2N)PP]VO generates a porphyrin π cation radical while subsequent oxidations involve reactions of DMF or one of the diethylamino groups for the case of [T(*p*-Et_2N)PP]VO. The effect of porphyrin ring structure on the redox reactions and electrode mechanisms of each complex in DMF is discussed.

Introduction

Both vanadyl and nickel porphyrins are widely distributed in natural petroleum and shale.[2] Trace amounts of vanadium are also found in some biological systems, and certain organisms can concentrate vanadium to an extraordinary degree. However, the manner in which vanadium affects living systems is largely unknown.

In a previous paper, we presented the electrochemistry of three Ni porphyrins of the form (TpyP)Ni, [T(*p*-SO_3Na)PP]Ni, and [T(*p*-Et_2N)PP]Ni.[3] The present work describes the electrochemical and spectroelectrochemical properties of vanadyl porphyrin complexes with the same porphyrin ring structures. The investigated vanadyl(IV) porphyrins are (TpyP)VO, [T(*p*-SO_3Na)PP]VO, and [T(*p*-Et_2N)PP]VO, whose structures are shown in Figure 1.

For some time the known electrochemistry of vanadium porphyrins had been restricted to that of vanadyl complexes of the type (OEP)VO[2-5] and [T(*p*-X)PP]VO.[4,6,7] However, dihalogenovanadium(IV) porphyrins[7] and vanadium(II) porphyrins[8] have recently been synthesized[9] and electrochemically characterized.[10]

This present study expands the type and number of complexes that have been investigated and provides an opportunity to better understand how the central metal ions of (P)VO and (P)Ni influence the redox behavior of two metalloporphyrins having the same porphyrin macrocycle. There is a difference between nickel(II) and vanadium(IV) regarding the number of d electrons in the outer configuration. Nickel(II) has eight d electrons and filled d_{xy}, d_{xz}, and d_{yz} orbitals, which can interact with the porphyrin π- or π^*-ring system. In contrast, vanadium has only one electron in the d_{xy} orbital and the d_{xz} and d_{yz} orbitals are empty. These differences, along with differences in porphyrin ring basicity of the TpyP, T(*p*-SO_3Na)PP, and T(*p*-Et_2N)PP macrocycles, are reflected in variations of both the redox potentials and the axial ligation reactions of the various complexes.

Experimental Section

Chemicals. *N,N*-Dimethylformamide (DMF), obtained from Eastman Chemicals, was vacuum-distilled twice over molecular sieves prior to use. Tetrabutylammonium perchlorate (TBAP) was purchased from Fluka Chemical Co., recrystallized from absolute ethanol, and dried under reduced pressure for at least 7 days prior to use. The concentration of TBAP was 0.2 M for controlled-potential electrolysis and spectroelectrochemical measurements and 0.1 M for polarographic and voltammetric measurements.

Synthesis of the three investigated porphyrins is described below:

(TpyP)VO. One gram of $(TpyP)H_2$ and 1.27 g of VCl_3 were refluxed in 350 mL of benzonitrile. After rapid evaporation of the solvent, the precipitated product was dissolved in CH_2Cl_2 and the mixture was washed with water and dried by $MgSO_4$. The resulting (TpyP)VO was washed with hexane, dried, and recrystallized from DMF to give a yield of about 35%. UV-visible data for (TpyP)VO in CH_2Cl_2 [λ_{max}, nm (ϵ)]: 420 (465.2×10^3), 541 (17.0×10^3), 578 (1.7×10^3).

[T(*p*-SO_3Na)PP]VO. Two grams of [T(*p*-SO_3NH_4)PP]H_2 and 1.57 g of VCl_3 were refluxed in 100 mL of DMF for 6 h. After evaporation of DMF, the mixture was dissolved in methanol. The resulting solution was filtered, and the obtained solid compound was washed with hexane and dried under vacuum. UV-visible data for [T(*p*-SO_3NH_4)PP]VO in water [λ_{max}, nm (ϵ)]: 434 (169.9×10^3), 562 (13.5×10^3), 602 (5.1×10^3). This complex was converted to [T(*p*-SO_3Na)PP]VO by passage through a column of Amberlite CG120, 100–200 mesh, sodium form.

[T(*p*-Et_2N)PP]VO. Two grams of [T(*p*-Et_2N)PP]H_2 and 1.87 g of VCl_3 were refluxed in 650 mL of DMF for 7 h. After evaporation of the solvent, the product was dissolved in CH_2Cl_2 and the mixture was washed with water in order to remove unreacted VCl_3. The resulting porphyrin was dried by $MgSO_4$, and the obtained crystals were washed with hexane and dried under vacuum. The yield for metalation was about 89%. UV-visible data for [T(*p*-Et_2N)PP]VO in CH_2Cl_2 [λ_{max}, nm (ϵ)]: 398 (43.5×10^3), 455 (152×10^3), 561 (17.3×10^3), 611 (22.7×10^3). References for synthesis of $(TpyP)H_2$, [T(*p*-SO_3NH_4)PP]H_2, and [T(*p*-Et_2N)PP]H_2 are given in a previous paper.[3]

Instrumentation and Methods. Cyclic voltammetry and polarography were carried out with a Princeton Applied Research EG&G Model 174 polarographic analyzer, coupled with a PAR 175 universal programmer, an IBM Instrument Model EC 225 voltammetric analyzer, or a BAS-100 electrochemistry system.

A three-electrode system was used for all experiments. The reference electrode was an aqueous saturated calomel electrode (SCE), which was separated from the bulk solution by a glassy diaphragm connected to a bridge filled with the electrolyte solution. The working electrode was a platinum button with a geometric area of 0.8 mm^2. A platinum wire was used as the counter electrode.

Thin-layer spectroelectrochemical measurements were obtained with an IBM Model EC 225 voltammetric analyzer that was coupled with a Tracor Northern TN-1710 multichannel analyzer and a TN-1710-24 floppy-disk system for spectral acquisitions. The thin-layer cell utilized

(1) (a) University of Houston. (b) Université Mohammed V. (c) Université de Dijon.
(2) Baker, E. W.; Palmer, S. E. In *The Porphyrins*; Dolphin, D., Ed.; Academic: New York, 1979; Vol. 1A, p 486.
(3) Kadish, K. M.; Sazou, D.; Liu, Y. M.; Saoiabi, A.; Fehrat, M.; Guilard, R. *Inorg. Chem.* **1988**, *27*, 1198.
(4) Kadish, K. M. *Prog. Inorg. Chem.* **1986**, *34*, 435–605.
(5) Fuhrhop, J. H.; Kadish, K. M.; Davis, D. G. *J. Am. Chem. Soc.* **1973**, *95*, 5140.
(6) Kadish, K. M.; Morrison, M. M. *Bioinorg. Chem.* **1977**, *7*, 107.
(7) Richard, P.; Poncet, J. L.; Barbe, J. M.; Guilard, R.; Goulon, J.; Rinaldi, D.; Cartier, A.; Tola, P. *J. Chem. Soc., Dalton Trans.* **1982**, 1451.
(8) Oumous, H.; Lecomte, C.; Protas, J.; Poncet, J. L.; Barbe, J. M.; Guilard, R. *J. Chem. Soc., Dalton Trans.* **1984**, 2677.
(9) Guilard, R.; Lecomte, C. *Coord. Chem. Rev.* **1985**, *65*, 98.
(10) Reeb, P.; Mugnier, Y.; Guilard, R.; Laviron, E. *Inorg. Chem.* **1987**, *26*, 209.

0020-1669/88/1327-2313$01.50/0

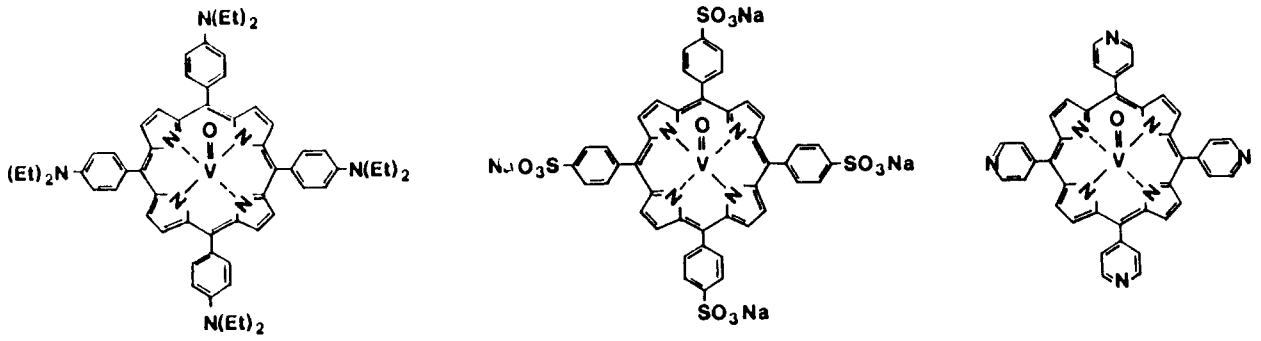

Figure 1. Structures of the investigated vanadyl porphyrins.

Table I. ESR Data for Neutral (P)VO Complexes

complex	solvent	g_{iso}	$g_{\parallel}$	$g_{\perp}$	A_{iso}, G	$A_{\parallel}$, G	$A_{\perp}$, G
(TpyP)VO	CH_2Cl_2	1.9807	1.9649	1.9792	96.88	171.84	58.71
	DMF	1.9801	1.9616	1.9822	92.96	171.82	59.20
$[(TpyP)VO]^-$	DMF		1.9653	1.9785		170.00	57.66
$[(TpyP)VO]^{2-}$	DMF		1.9616	1.9795		171.33	58.66
[T(*p*-SO_3Na)PP]VO	DMF	1.9869	1.9644	1.9815	80.00	171.18	58.18
[T(*p*-Et_2N)PP]VO	CH_2Cl_2	1.9798	1.9612	1.9807	94.53	171.38	59.34
	DMF	1.9811	1.9600	1.9788	92.64	171.33	57.40

a doublet platinum-gauze working electrode and has been described in the literature.[11]

UV–visible spectra of the neutral complexes were obtained with an IBM Model 9430 UV–visible spectrophotometer. Matched quartz cells with 1.0- or 0.1-cm path lengths were used for these measurements.

ESR spectra were recorded either on an IBM Model ER 100-D spectrometer or on a Bruker ESP 300 spectrometer interfaced with an Aspect 2000/3000 computer. Low temperature was achieved with a stream of nitrogen cooled by a heat exchanger immersed in liquid nitrogen. g values were calculated by calibration with diphenylpicrylhydrazyl (DPPH). The ESR signal of this compound is at $g = 2.0036 \pm 0.0003$. ESR spectra were simulated on a MINC-11 computer from the Digital Equipment Corp. The simulation program is described in ref 12.

Results and Discussion

ESR and UV–Visible Data for the Neutral (P)VO Complexes. Room-temperature and low-temperature ESR data for the three investigated (P)VO complexes in DMF and CH_2Cl_2 are given in Table I. The observed parameters are characteristic of a d^1 V(IV) nucleus.[13] At room temperature, the (P)VO complexes each exhibit an eight-line ESR spectrum centered at $g \approx 1.98$. The spectrum has an isotropic coupling constant that varies from 80.00 to 96.88 G. There is a significant difference between the coupling constants in CH_2Cl_2 and DMF for (TpyP)VO and [(T(*p*-Et_2N)PP]VO, and the decrease in coupling constant for these two complexes upon going from CH_2Cl_2 to DMF is consistent with an axial coordination of DMF at room temperature.

The UV–visible data for the three complexes also indicate coordination of DMF by (TpyP)VO and [T(*p*-SO_3Na)PP]VO at room temperature. The axial complexation of (TPP)VO and [T(*p*-X)PP]VO by various ligands, L, is uncomplicated and proceeds in nonbonding solvents as shown in eq 1, where P rep-

$$(P)VO + L \rightleftharpoons (P)VO(L) \qquad (1)$$

resents the T(*p*-X)PP[14] or TPP[15] macrocycle. (TPP)VO has absorption bands at 423 and 547 nm in CH_2Cl_2. These bands are red-shifted by 10–15 nm upon formation of (P)VO(L) and, for the specific case of (TPP)VO(Me_2SO) in CH_2Cl_2, are located at 436 and 562 nm.[15] There is a third absorption band for (TPP)VO(L), which for the case of (TPP)VO(Me_2SO) is located at 602 nm.

Similar types of spectral changes are observed during complexation of [T(*p*-SO_3Na)PP]VO or (TpyP)VO by DMF. For example, (TpyP)VO absorbs at 420 and 541 nm in CH_2Cl_2 containing 5% DMF but at 420, 431, and 558 nm in neat DMF. There is a red shift of the (TpyP)VO peaks upon increasing the DMF ratio in a mixed CH_2Cl_2/DMF solvent, and an isosbestic point is observed at 426 nm. This is illustrated in Figure 2.

Figure 2 also illustrates the spectral changes of [T(*p*-SO_3Na)PP]VO and [T(*p*-Et_2)PP]VO as the DMF concentration is increased in a CH_2Cl_2/DMF mixture. The [T(*p*-SO_3Na)-PP]VO complex absorbs at 424 and 548 nm in CH_2Cl_2 containing 5% DMF and at 424, 434, and 550 nm in neat DMF. An isosbestic point is located at 430 nm. These spectral data clearly indicate that [T(*p*-SO_3Na)PP]VO is complexed by a DMF molecule, as shown by eq 1. On the other hand, the spectra of [T(*p*-Et_2N)PP]VO are similar in both CH_2Cl_2 and DMF, thus suggesting that this vanadyl complex does not axially coordinate with a DMF solvent molecule at room temperature.

Formation constants for DMF binding by (TpyP)VO and [T-(*p*-SO_3Na)PP]VO in CH_2Cl_2 were calculated at 23 ± 1 °C (according to eq 1) by analysis of the spectral data[16] and gave values of 0.090 and 0.068, respectively. These values may be compared to a DMF binding constant of 0.018 for (TPP)VO in CH_2Cl_2 (this study) and are consistent with the small binding constants ($K < 2$) calculated for complexation of different (P)VO complexes by Lewis bases in nonbonding solvents.[14,15]

Electrochemistry of (TpyP)VO(DMF). The reduction of (TpyP)VO(DMF) is characterized by reversible processes at $E_{1/2} = -0.82$ and -1.27 V in DMF. These reductions are labeled as processes I and II in Figure 3. No other oxidations or reductions are observed in DMF between the potentials of −2.0 and +1.4 V vs SCE.

The cyclic voltammetric peak currents for processes I and II increase linearly with $v^{1/2}$, and the half-wave potentials are independent of potential scan rate. The peak shapes are charac-

(11) Lin, X. Q.; Kadish, K. M. *Anal. Chem.* **1985**, *57*, 1498.
(12) Richard, R. Thesis, Université de Dijon, 1982.
(13) Poncet, J. L.; Guilard, R.; Friant, P.; Goulon-Ginet, C.; Goulon, J. *Nouv. J. Chem.* **1984**, *8*, 583.
(14) Walker, F. A.; Hui, E.; Walker, J. M. *J. Am. Chem. Soc.* **1975**, *97*, 2390.
(15) Bencosme, S.; Romero, C.; Simoni, S. *Inorg. Chem.* **1985**, *24*, 1603.
(16) Formation constants for DMF addition to (P)VO were determined by changes in the Soret-band intensity of the porphyrin as a function of DMF concentration in seven or more different CH_2Cl_2/DMF mixtures at 23 ± 1 °C. Calculations were carried out according to Ketelaar's method.[17]
(17) Ketelaar, J. A.; van de Stolpe, C.; Doudsmit, A.; Dzcubas, W. *Recl. Trav. Chim. Pays-Bas* **1952**, *71*, 1104.

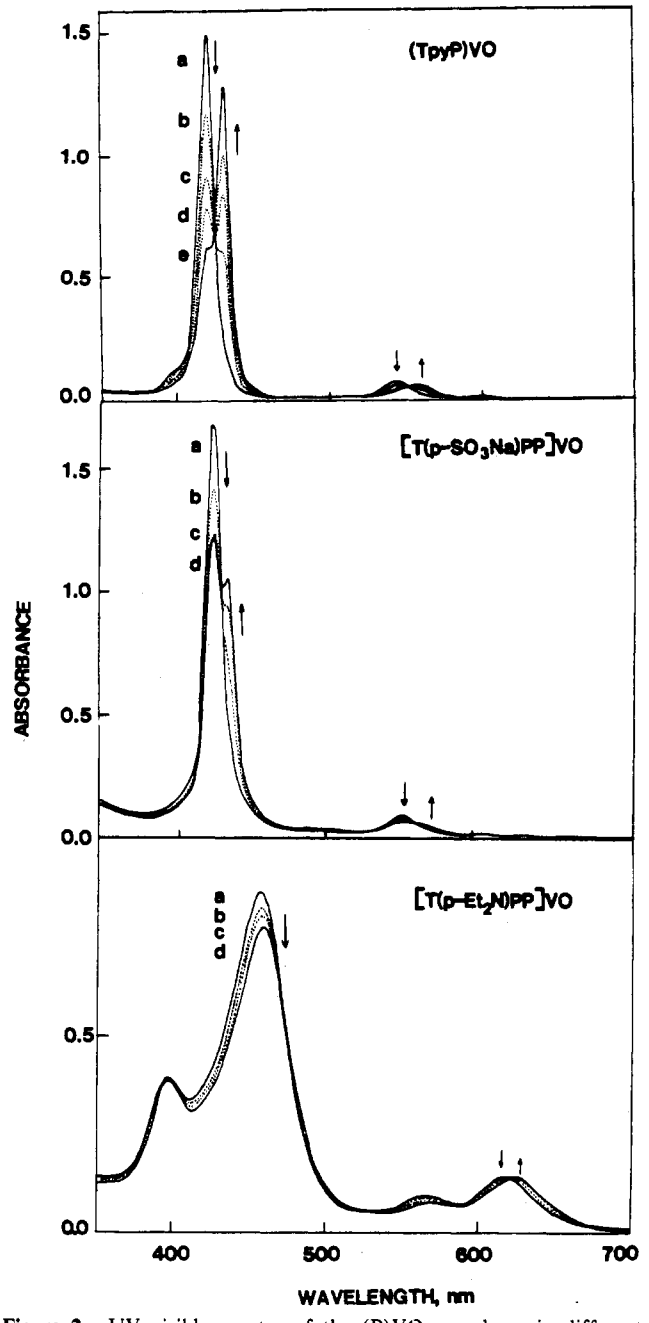

Figure 2. UV–visible spectra of the (P)VO complexes in different CH_2Cl_2 mixtures at 23 ± 1 °C. Mole percent of DMF is as follows. (TpyP)VO: (a) 2%; (b) 37%; (c) 46%; (d) 67%; (e) 100%. [T(*p*-SO_3Na)PP]VO: (a) 7.7%; (b) 41%; (c) 71%; (d) 100%. [T(*p*-Et_2N)-PP]VO: (a) 0%; (b) 19%; (c) 57%; (d) 100%. Arrows indicate the direction of spectral changes upon going from solution a to solution e.

terized by $|E_{pc} - E_{pa}| = 60 \pm 5$ mV at scan rates up to 0.5 V/s. These values agree with theoretical values for diffusion-controlled one-electron transfers, and this was verified by controlled-potential electrolysis, which gave 1.0 ± 0.2 electrons for each reduction step.

The absolute potential difference between processes I and II is 0.44 V, which is within the range of 0.45 ± 0.05 V observed for the two successive reductions of different octaethyl- or tetraphenylporphyrins at the π-ring system.[4,5] The formation of a porphyrin π anion radical is also demonstrated by ESR and electronic absorption spectra recorded during stepwise controlled-potential reduction of (TpyP)VO(DMF). These latter spectra are shown in Figure 4, and UV–visible spectral data for the neutral and the reduced forms of the complex are summarized in Table II.

After addition of one electron to (TpyP)VO(DMF), the Soret band at 431 nm decreases in intensity and shifts to 443 nm. The

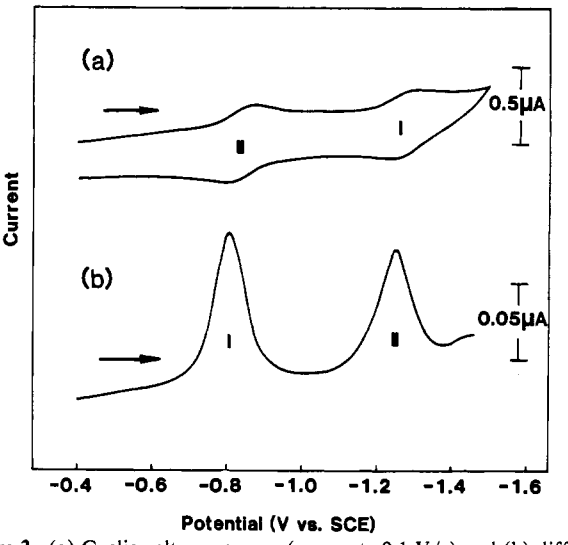

Figure 3. (a) Cyclic voltammogram (scan rate 0.1 V/s) and (b) differential-pulse voltammogram (pulse width 0.04 V, scan rate 0.05 V/s) of 9.7×10^{-4} M (TpyP)VO(DMF) in DMF, 0.1 M TBAP.

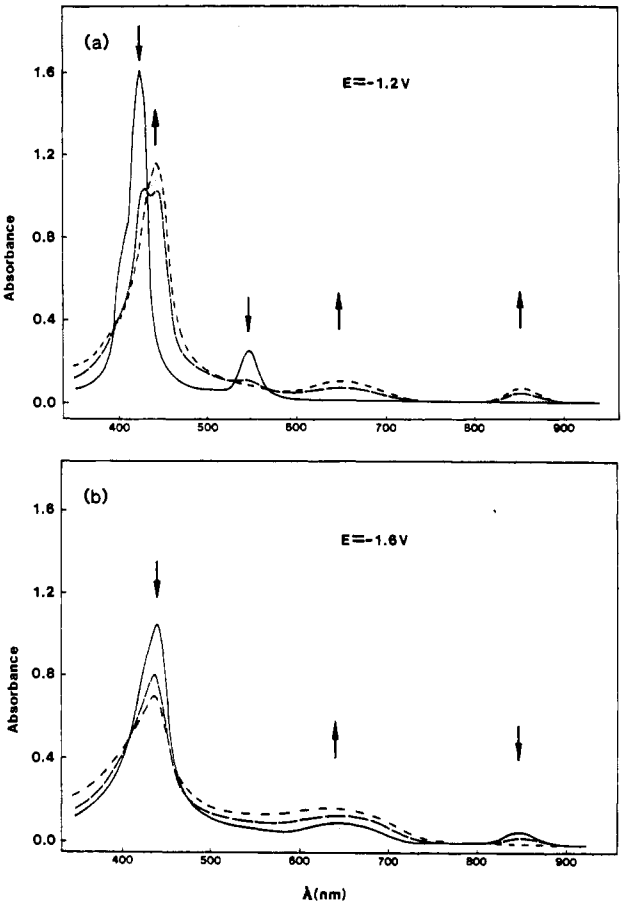

Figure 4. Time-resolved thin-layer electronic absorption spectra obtained during controlled-potential reduction of 2.63×10^{-4} M (TpyP)VO(DMF) at (a) −1.2 V and (b) −1.6 V in DMF, 0.2 M TBAP. Arrows indicate the direction of spectral changes during electroreduction.

final product of the first electroreduction has a broad absorption band centered at 669 nm and a characteristic π-anion-radical absorption peak at 854 nm. These changes are shown in Figure 4a. The final spectrum of the doubly reduced complex has a Soret band at 442 nm and another band at 669 nm. This spectrum is shown in Figure 4b and is characteristic of a porphyrin dianion.

The ESR data are consistent with the UV–visible data with respect to characterizing the site of electroreduction. The neutral (TpyP)VO complex has an eight-line ESR spectrum centered at $g \approx 1.98$ (Figure 5a). The V(IV) signal decreases in intensity

Table II. Absorption Maxima and Molar Absorptivities for Investigated Vanadyl Porphyrins in DMF

porphyrin ring	reacn	λ_{max}, nm ($10^{-3}\epsilon$, cm^{-1} M^{-1})						
TpyP	neutral	420 (161.0)	431 (362.0)		558 (13.7)	597 (2.9)		
	redn 1		443 (262.8)			669 (24.8)		854 (14.9)
	redn 2		442 (158.0)			669 (39.0)		
T(p-SO_3Na)PP	neutral		424 (2.3.0)	434 (220.0)	550 (9.4)	600 (2.3)		
	redn 1		430 (119.7)	436 (110.0)		680 (6.5)		850 (12.9)
	redn 2		457 (80.9)			600 (12.9)		
	oxidn 1		428 (93.0)	436 (90.6)		650 (16.2)		
	oxidn 2		430 (14.3)	436 (111.0)				870 (12.0)
T(p-Et_2N)PP	neutral	398 (40.9)	457 (98.6)		570 (4.8)	626 (15.0)		
	redn 1		475 (93.7)				712 (7.2)	856 (4.8)
	redn 2		453 (79.3)		563 (12.0)	613 (14.4)		
	oxidn 1		450 (57.7)	498 (62.5)	563 (38.5)			813 (21.6)
	oxidn 2	398 (69.7)	467 (33.6)		510 (24.0)		>725 (15.6)	

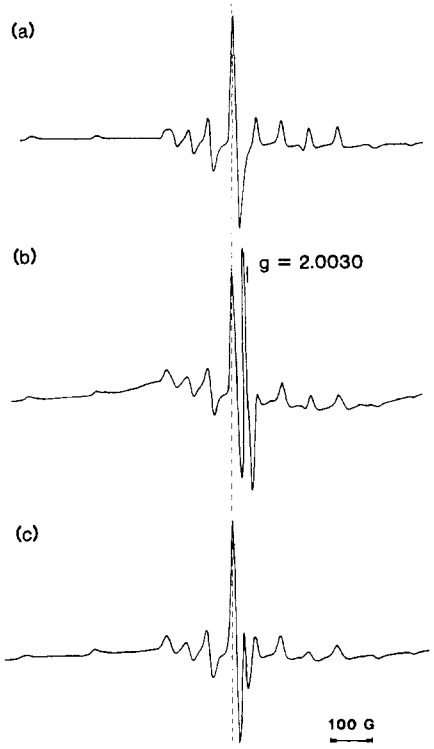

Figure 5. ESR spectra at 77 K (a) of (TpyP)VO before electrolysis, (b) of $[(TpyP)VO]^-$ generated by controlled-potential reduction at −1.1 V, and (c) of $[(TpyP)VO]^{2-}$ generated by controlled-potential reduction at −1.5 V.

but does not disappear after addition of one electron to the complex, and the spectrum is then characterized by a strong radical signal centered at $g = 2.003$ (see Figure 5b). This change in the ESR spectrum suggests the formation of a porphyrin π anion radical and a lack of coupling between the odd electron on the metal and that on the reduced macrocycle of $[(TpyP)VO]^-$. The addition of a second electron to $[(TpyP)VO]^-$ results in a loss of the porphyrin radical signal, and the reappearance of a strong V(IV) signal as $[(TpyP)VO]^{2-}$ is generated (see Figure 5c). Thus, the electrochemical, spectroelectrochemical, and ESR data are all consistent with π-anion-radical and dianion generation during electroreduction of (TpyP)VO(DMF).

DMF remains complexed to (TpyP)VO after electroreduction in DMF. This was determined by monitoring the $E_{1/2}$ values for reduction of this complex in solutions containing various proportions of CH_2Cl_2 and DMF. In the classical electrochemical evaluation of ligand binding by metalloporphyrins, values of $E_{1/2}$ are plotted as a logarithmic function of the ligand concentration.[18-20] The results obtained by this type of electrochemical

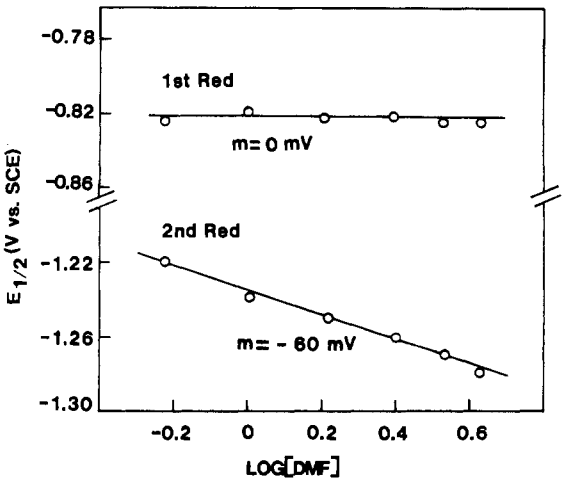

Figure 6. Plots of $E_{1/2}$ vs log [DMF] for the two reductions of 6×10^{-4} M (TpyP)VO in CH_2Cl_2/DMF mixtures containing 0.1 M TBAP.

evaluation are generally quite conclusive for the case of metalloporphyrin ligand binding and in addition will often provide formation constants within experimental error of those determined by using spectral methodologies.

(TpyP)VO is reversibly reduced via two steps in solutions containing either neat DMF or a mixture of DMF and CH_2Cl_2. The first reduction occurs at $E_{1/2} = -0.83$ V, independent of the DMF concentration. In contrast, the second reduction of (TpyP)VO(DMF) shifts by -60 ± 5 mV per decadic increase in log [DMF]. These data are shown in Figure 6 and are consistent with the series of electron-transfer steps given by eq 2 and 3, where P = TpyP.

$$(P)VO(DMF) + e^- \rightleftarrows [(P)VO(DMF)]^- \quad (2)$$

$$[(P)VO(DMF)]^- + e^- \rightleftarrows [(P)VO]^{2-} + DMF \quad (3)$$

The initial binding of DMF by (TpyP)VO occurs as shown in eq 1 when the concentration of DMF is about 0.6 M. This DMF ligand is not lost after the addition of the first electron (eq 2) but rather after the formation of $[(TpyP)VO]^{2-}$ (eq 3). The −60-mV shift of $E_{1/2}$ for this reaction can only be accounted for by loss of a single DMF molecule after electroreduction. An oxo group occupies one site on (P)VO(DMF) so that the shifts of $E_{1/2}$ are uniquely assigned to the electrode reactions given in eq 2 and 3. Finally, the formation constant for DMF binding to $[(TpyP)VO]^-$ was calculated as 0.58 from the voltammetric data in Figure 6.

Electrochemistry of [T(p-SO_3Na)PP]VO(DMF). Cyclic voltammograms of [T(p-SO_3Na)PP]VO(DMF) in DMF at several temperatures are shown in Figure 7. At room temperature [T(p-SO_3Na)PP]VO(DMF) is reduced at $E_{1/2} = -0.96$ and -1.48 V. The absolute potential difference between these two reductions is close to the 0.45 ± 0.05 V separation predicted for subsequent addition of two electrons to the porphyrin π-ring system of different

(18) Kadish, K. M. In *Iron Porphyrins*; Lever, A. B. P., Gray, H. B., Eds.; Addison-Wesley, Reading, MA, 1983; Part 2, pp 161-249.
(19) Kelly, S. L.; Kadish, K. M. *Inorg. Chem.* **1984**, *23*, 679.
(20) Kadish, K. M.; Shiue, L. R. *Inorg. Chem.* **1982**, *21*, 3623.

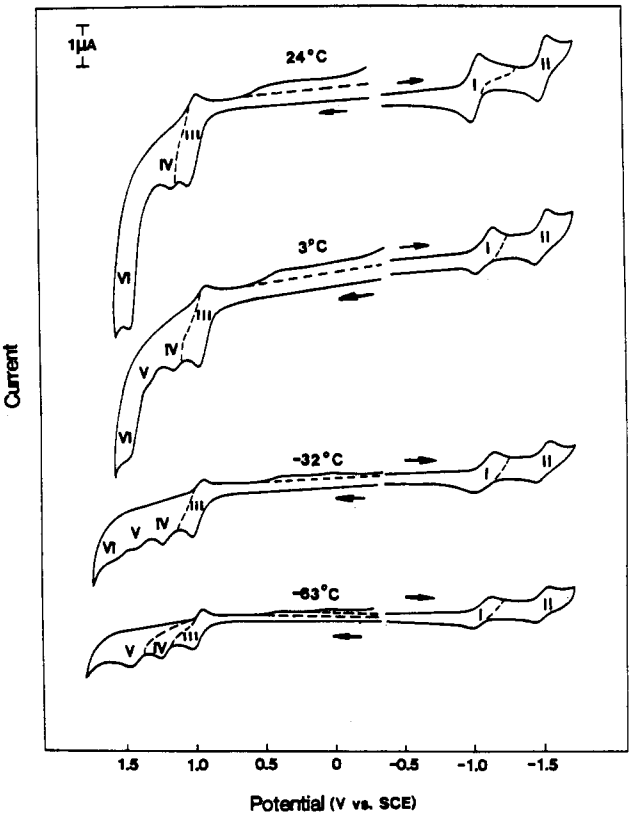

Figure 7. Cyclic voltammograms of 9.95×10^{-4} M [T(*p*-SO_3Na)PP]-VO(DMF) at different temperatures in DMF, 0.1 M TBAP (scan rate 0.2 V/s).

metalloporphyrin complexes.[4] Controlled-potential electrolysis at −0.96 and −1.48 V gave 0.9 and 1.1 electrons, respectively, and confirms the addition of one electron in each reduction step. The values of $i_p/v^{1/2}$ are independent of potential scan rate from 0.02 to 0.80 V/s, indicating diffusion-controlled processes. The peak separations $|E_{pa} - E_{pc}|$ and $|E_p - E_{p/2}|$ are between 66 and 70 mV and are slightly larger than theoretical values of 59 mV for a one-electron-transfer process.

Values of $E_{1/2}$ were also monitored as a function of DMF concentrations and gave plots similar to the type shown in Figure 6. The first reduction was invariant with changes in the DMF/CH_2Cl_2 ratio while the second reduction shifted by −60 mV per 10-fold increase in log (DMF). These data indicate a loss of bound DMF after formation of the dianion and are uniquely consistent with the type of electrode reactions given by eq 2 and 3. It should also be noted that Na^+ ions do not completely dissociate from the T(*p*-SO_3Na)PP macrocycle in DMF solutions. Conductivity measurements show that the singly ionized form of [T(*p*-SO_3Na)PP]VO is predominant in solution. The measured molar conductivity of [T(*p*-SO_3Na)PP]VO in DMF is 33.90 mhos mol^{-1} cm^2, while that of TBAP is 38.6 mhos mol^{-1} cm^2 in the same solution. This suggests that less than one-fourth of the Na^+ ions on [T(*p*-SO_3Na)PP]VO are dissociated in DMF.

[T(*p*-SO_3Na)PP]VO(DMF) is oxidized at room temperature at $E_{1/2}$ = 1.02 V (process III) and E_p = 1.45 V (process VI). There is also an oxidation peak IV that is overlapped with process III. Controlled-potential oxidation of [T(*p*-SO_3Na)PP]VO(DMF) at 1.1 V gives 2.7 electrons for the combined oxidation processes III and IV. On the other hand, controlled-potential electrolysis at a potential positive of 1.1 V gives a much larger number of electrons.

The relationship between i_p and $v^{1/2}$ for peak VI deviates from linearity at room temperature, and this suggests either a kinetic

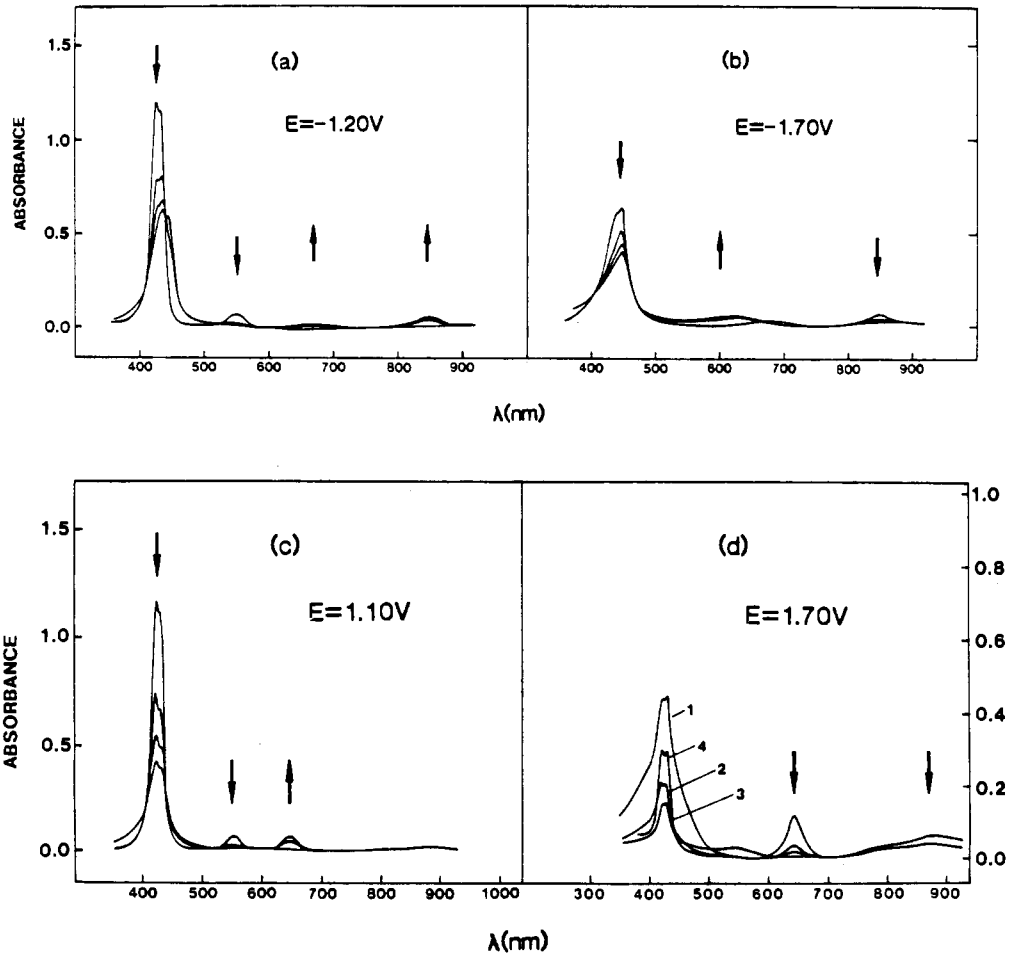

Figure 8. Time-resolved thin-layer electronic absorption spectra of 1.14×10^{-4} M [T(*p*-SO_3Na)PP]VO in DMF, 0.2 M TBAP obtained during controlled-potential electrolysis at (a) −1.2 V, (b) −1.7 V, (c) 1.1 V, and (d) 1.7 V.

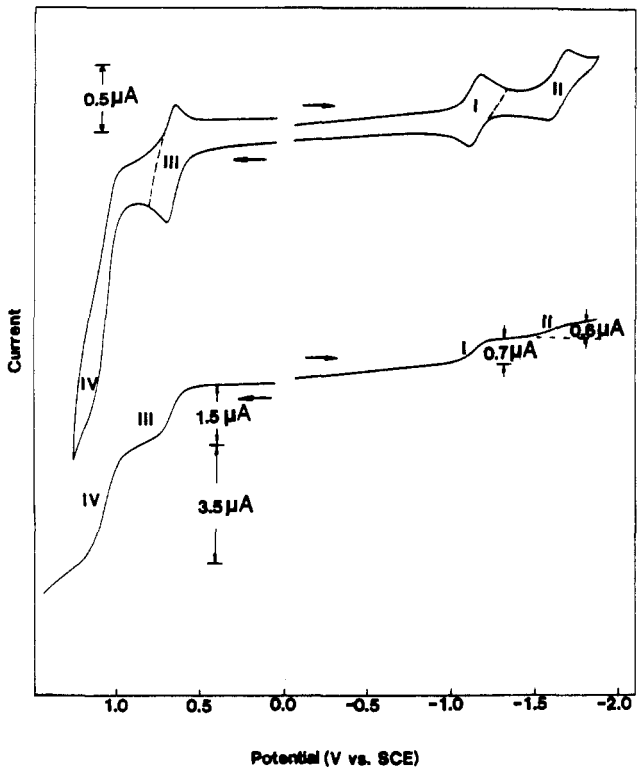

Figure 9. Cyclic voltammogram (scan rate 0.1 V/s) and rotating-disk voltammogram (rotation rate 750 rpm) of 8.8×10^{-4} M [T(*p*-Et_2N)PP]VO in DMF, 0.1 M TBAP.

or a catalytic controlled process. At −63 °C oxidation peaks IV and V are irreversible but still involve a one-electron oxidation. Oxidation peak III invariably involves a two-electron-transfer process at all temperatures.

The spectral changes that occur during controlled-potential reduction and oxidation of [T(*p*-SO_3Na)PP]VO(DMF) are shown in Figure 8. A new peak appears at 850 nm during the addition of one electron and implies π-anion-radical formation. This absorbance decreases and disappears when the applied potential is set to −1.7 V and is consistent with dianion formation. This spectrum is shown in Figure 8b.

Spectral changes during oxidation of [T(*p*-SO_3Na)PP]VO(DMF) at 1.1 and 1.7 V are presented in Figure 8c,d. After the first oxidation (Figure 8c) there is a considerable decrease of both the Soret-band and the Q-band absorption intensities. No absorbance bands in the range 800–900 nm can be assigned to π-cation-radical formation, but a broad band appears in this range after thin-layer electrolysis at slightly more positive potentials (these spectra are not shown in Figure 8). When the applied potential is set to 1.7 V, both the broad band and the new band at 650 nm decrease (Figure 8d). The Soret band initially decreases but then increases again, thus suggesting regeneration of the initial form. These time-resolved spectral changes are consistent with a catalytic oxidation of DMF that occurs in the presence of the porphyrin cation radical.[21,22]

The potentials for oxidation of an axial DMF ligand and that for oxidation of free DMF overlap at room temperature. However, at lower temperature these oxidations are separated and are labeled as wave V and wave VI. At −63 °C, oxidation process VI involves a one-electron-transfer process, but even at this temperature, it is coupled to a rereduction at +0.3 V. This peak is due to the reduction of protons produced during oxidation of DMF.[21]

Electrochemistry of [T(*p*-Et_2N)PP]VO. Figure 9 shows a cyclic voltammogram and rotating-disk-electrode voltammogram of [T(*p*-Et_2N)PP]VO in DMF. The complex undergoes reductions

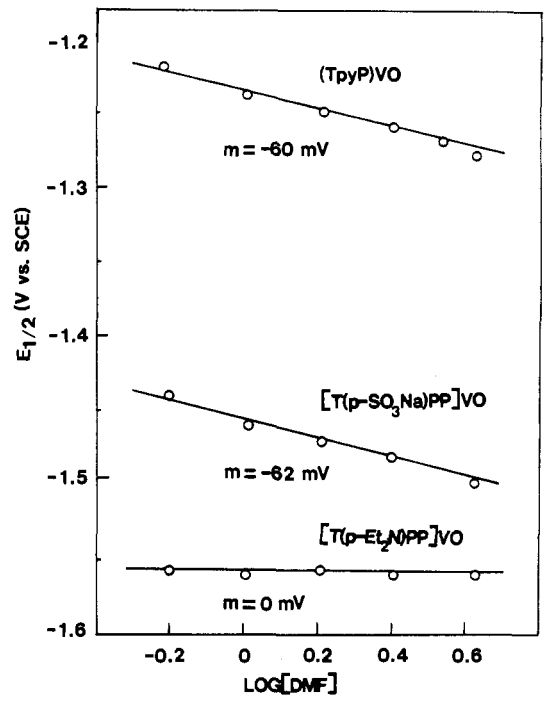

Figure 10. Dependence of $E_{1/2}$ on DMF concentration for the second reduction of the (P)VO complexes in CH_2Cl_2.

at $E_{1/2}$ = −1.08 and −1.57 V and oxidations at $E_{1/2}$ = 0.68 V and E_p = 1.04 V. Reduction waves I and II are diffusion controlled, as verified by the constant values of $i_p/v^{1/2}$ and the invariant $E_{1/2}$ values with increase in potential sweep rate. The potential difference between the cathodic and anodic reduction peaks, $|E_{pc} - E_{pa}|$, is equal to 60 ± 5 mV and thus indicates that each reduction involves a reversible one-electron addition.

A DMF solvent molecule does not coordinate to [T(*p*-Et_2N)PP]VO. This is evident from both spectrally and electrochemically monitored titrations of the neutral complex in CH_2Cl_2 with DMF. The coupling constants in the ESR spectra of the neutral complex are similar in CH_2Cl_2 and DMF (see Table I), as are the UV–visible spectra of the complex in these two solvents (see Figure 2). Both of these results contrast with the results for (TpyP)VO, which has a 4-G decrease in coupling constant and an 11-nm difference in absorption peaks between CH_2Cl_2 and DMF. In addition, there is no $E_{1/2}$ dependence on DMF concentration for the first or second reduction of [T(*p*-Et_2N)PP]VO in CH_2Cl_2/DMF mixtures. These electrochemical data are shown in Figure 10, which illustrates the $E_{1/2}$ dependence on DMF for the second reduction of all three complexes and gives unambiguous evidence for the lack of DMF complexation by [T(*p*-Et_2N)PP]VO at room temperature.

The first oxidation of [T(*p*-Et_2N)PP]VO (see Figure 9) is reversible and diffusion controlled. There is a linear relationship between i_p and $v^{1/2}$, but the peak separations $|E_p - E_{p/2}|$ and $|E_{pa} - E_{pc}|$ are equal to 45 ± 5 mV, which is larger than the values expected for a two-electron-transfer process. However, the limiting first oxidation current by rotating-disk voltammetry (1.5 μA) is approximately twice that of the limiting first reduction current (0.7 μA), and this also suggests a two-electron oxidation process. The second oxidation of [T(*p*-Et_2N)PP]VO involves a multielectron irreversible process at room and higher temperatures. The process is not diffusion controlled since i_p is not linearly dependent on $v^{1/2}$.

It is known that tertiary aromatic amines can be oxidized in aprotic media to initially give a monocation radical.[23,24] The four

(21) Ross, S. D.; Finkelstein,M.; Petersen, R. C. *J. Am. Chem. Soc.* **1966**, *88*, 4657.
(22) Mann, C. K.; Barnes, K. K. *Electrochemical Reactions in Nonaqueous Systems*; Marcel Dekker: New York, 1970; p 287.
(23) Nelson, R. C.; Adams, R. N. *J. Electroanal. Chem. Interfacial Electrochem.* **1968**, *16*, 439.
(24) Seo, E. T.; Nelson, R. F.; Fritsch, J. M.; Marcous, L. S.; Leedy, D. W.; Adams, R. N. *J. Am. Chem. Soc.* **1966**, *88*, 3438.
(25) Williams, R. F. X.; Hambright, P. *Bioinorg. Chem.* **1978**, *9*, 537.

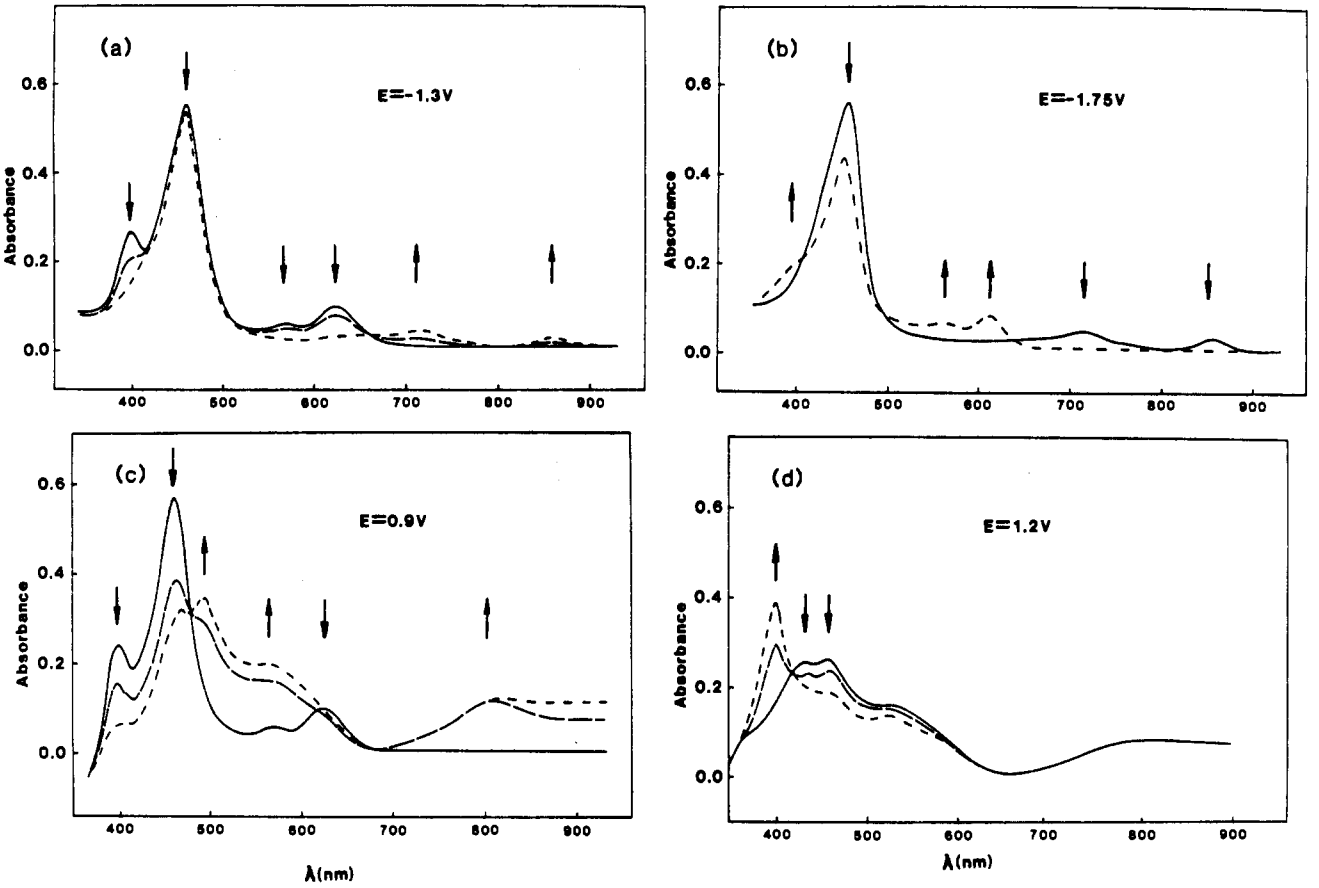

Figure 11. Time-resolved electronic absorption spectra during thin-layer electrolysis of 2.93×10^{-4} M [T(p-Et_2N)PP]VO at (a) −1.3 V, (b) −1.75 V, (c) 0.9 V, and (d) 1.2 V.

Table III. Half-Wave Potentials and Number of Electrons Transferred during Each Electrode Reaction of (P)VO in DMF, 0.1 M TBAP

	$E_{1/2}$, V vs SCE (no. of electrons transferred)[a]				
	redn			oxidn	
complex	1st	2nd	3rd	1st	2nd
(TpyP)VO	−0.83 (1)	−1.27 (1)			
[T(p-SO_3Na)PP]VO	−0.96 (1)	−1.48 (1)		1.02 (2)	1.45[b]
(TPP)VO	−0.98 (1)	−1.50 (1)		1.01 (1)	1.32 (1)
[T(p-Et_2N)PP]VO	−1.08 (1)	−1.57 (1)		0.68 (2)	1.04[b]

[a] Determined from analysis of current–voltage curve. [b] Peak potential, E_p, at a scan rate of 0.1 V/s.

diethylamino groups can be oxidized by four electrons to give the corresponding radicals. $(C_2H_5)_3N$ is irreversibly oxidized at about E_p = 1.45 V in DMF while $(C_2H_5)_2N(C_6H_4CHO)$ undergoes a reversible one-electron oxidation at $E_{1/2}$ = 1.4 V under the same solution conditions. Also a common characteristic of both the $(C_2H_5)_2N(C_6H_4CHO)$ and the porphyrin oxidation in DMF is the strong contamination of the electrode surface by the oxidation products.

The stepwise controlled-potential reduction and oxidation of [T(p-Et_2N)PP]VO were spectrally monitored, and the electronic absorption spectra obtained during electrolysis at the different potentials are shown in Figure 11. The singly reduced species is assigned as a porphyrin π anion radical in DMF. Support for a porphyrin ring reduction also comes from the potential difference between the two reduction waves. The experimentally estimated difference of $\Delta E_{1/2}$ = 0.49 ± 0.02 V agrees with the average value of 0.45 ± 0.05 V reported for two consecutive porphyrin ring reductions.[4]

Spectral changes during controlled-potential oxidation of [T(p-Et_2N)PP]VO at 0.9 and 1.2 V are shown in Figure 11c,d. The product of the first oxidation has a split Soret band at 450 and 498 nm. A single isosbestic point is observed at 482 nm. The product obtained after controlled-potential oxidation of [T(p-Et_2N)PP]VO at 0.9 V has an intense ESR signal at g = 1.980 and is characteristic of a V(IV) complex. Thus, the ESR results are consistent with the coulometric and voltammetric data, which clearly indicate a two-electron-transfer process in the first oxidation step.

Effect of Porphyrin Ring Basicity on Axial Ligation and Redox Reactions of (P)VO and (P)Ni in DMF. A DMF molecule is axially coordinated with (TpyP)VO and [T(p-SO_3Na)PP]VO in neat DMF, but no coordination reaction occurs in the case of [T(p-Et_2N)PP]VO. This demonstrates that axial ligation of (P)VO by DMF is dependent upon the basicity of the porphyrin macrocycle. The pyridyl and (p-SO_3Na)C_6H_4 meso substituents are electron-withdrawing and this contrasts with (p-Et_2N)C_6H_4, which is electron donating.

A summary of half-wave potentials for electrooxidation/reduction of the three investigated vanadyl porphyrins and of (TPP)VO is given in Table III. As expected, more difficult reductions are observed for the [T(p-Et_2N)PP]VO complex while easier reductions occur for the porphyrins that have more electropositive porphyrin macrocycles.[4] The substituent effect of the porphyrin ring may be correlated to $E_{1/2}$ through a substituent constant, σ, or in some cases other measures of porphyrin ring basicity may be utilized.[4]

One correlation that has been previously utilized involves a plot of $E_{1/2}$ for reduction of the metalloporphyrin vs $E_{1/2}$ for reduction of the free base complex.[25] This type of plot is illustrated in Figure 12 and clearly shows how the peripheral porphyrin ring substit-

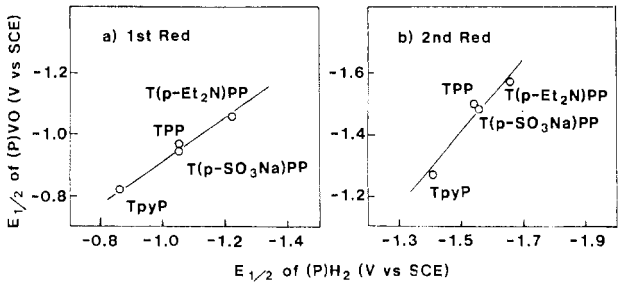

Figure 12. Correlation between half-wave potentials for the first and second reductions of the various vanadyl porphyrins versus half-wave potentials for reduction of the corresponding free-base complex in DMF.

uents affect the reduction potentials. $E_{1/2}$ values for both the first and the second reduction of the vanadyl porphyrins are plotted in Figure 12 against $E_{1/2}$ for the corresponding free-base porphyrin. A good linear relationship is obtained.

Redox potentials for the same series of Ni(II) porphyrins under the same solution conditions have also been measured.[3] Ni(II) has eight electrons in its outer configuration but contains a full complement of d electrons (four) that can interact with the π^* orbitals of the porphyrin. The V(IV) complexes contain only one electron in the d_{xy} orbital and cannot interact with the π^* orbitals of the porphyrin ring.[26]

The results in Figure 12 show that the electronic effect of the porphyrin ring substituents affect the redox potentials of the oxovanadium complexes to a smaller degree than those of the nickel complexes. However, these differences are not large and can be explained by the fact that the empty d_{xz} and d_{yz} orbitals of V(IV) have the proper symmetry for overlap with the filled π orbitals of the porphyrin ring and are lower in energy than the d orbitals of V(IV).

In summary, the porphyrin ring substituents have a strong influence on the redox potentials of both the nickel and the vanadyl complexes. The pyridyl electron-withdrawing substituent in the meso position of the porphyrin ring leads to easier reductions. At the same time the oxidation becomes more difficult.

Acknowledgment. The support of the National Science Foundation (Grant No. CHE-8515411) and the CNRS is gratefully acknowledged.

Registry No. (TpyP)VO, 58593-48-9; [T(*p*-SO_3Na)PP]VO, 93410-57-2; [T(*p*-Et_2N)PP]VO, 114466-58-9; DMF, 68-12-2; Pt, 7440-06-4; CH_2Cl_2, 75-09-2; (TpyP)VO(DMF), 114580-83-5; [T(*p*-SO_3Na)PP]-VO(DMF), 114580-84-6; [(TpyP)VO(DMF)]$^-$, 114594-55-7; [[T(*p*-SO_3Na)PP]VO(DMF)]$^-$, 114614-04-9; [(TpyP)VO]$^{2-}$, 114580-85-7; [[T(*p*-SO_3Na)PP]VO]$^{2-}$, 114580-86-8; [(TpyP)VO]$^-$, 114580-87-9.

(26) Smith, K. M. In *Porphyrins and Metalloporphyrins*; Smith, K. M., Ed.; Elsevier: New York, 1975.

Contribution from the Department of Chemistry, University of Houston, Houston, Texas 77004

Electrochemical Studies of Dimeric Rhodium(III) Porphyrins Containing a Dibasic Nitrogen-Heterocyclic Bridging Ligand

Y. H. Liu, J. E. Anderson, and K. M. Kadish*

Received January 11, 1988

The electrochemistry and spectroelectrochemistry of $[(P)RhCl]_2L$, where P is the dianion of tetraphenylporphyrin (TPP) or octaethylporphyrin (OEP) and L is a conjugated dibasic nitrogen-heterocyclic ligand such as 4,4′-bipyridine (bpy) or *trans*-1,2-bis(4-pyridyl)ethylene (BPE) or a nonconjugated nitrogen-heterocyclic ligand such as 1,2-bis(4-pyridyl)ethane (BPA) or 4,4′-trimethylenebis(pyridine) (TMDP), are reported. The Rh(III) dimers with BPA or TMDP nonconjugated bridging ligands undergo one irreversible metal-centered reduction in tetrahydrofuran or methylene chloride. However, two overlapping irreversible metal center reductions are observed for Rh(III) dimers that are linked via the conjugated bridging ligands, bpy and BPE. In all cases, $[(P)Rh]_2$ and the free nitrogen-heterocyclic ligand are generated as products from one or more chemical reactions that follow the metal-centered reduction of Rh(III) to Rh(II). Two reversible two-electron oxidations are observed for $[(P)RhCl]_2L$, where L = BPE, BPA, and TMDP. This contrasts with the case for $[(P)RhCl]_2$bpy, which undergoes a single reversible two-electron transfer followed by two reversible one-electron oxidations. On the basis of the electrochemical and spectroelectrochemical data, an overall mechanism for reduction and oxidation of the $[(P)RhCl]_2L$ complexes is presented.

Introduction

The electrochemistry of bridged iron porphyrins and iron phthalocyanines of the form $[(P)Fe]_2X$ and $[(Pc)Fe]_2X$, where Pc is the dianion of phthalocyanine, P is the dianion of a given porphyrin macrocycle, and X = C, N, or O, has been reported.[1-7] Multiple single-electron-transfer processes are observed for the above complexes in both the porphyrin and the phthalocyanine series, and this implies an interaction of the two macrocyclic units across the bridging atom. In contrast, replacement of the single-atom bridge in $[(P)Fe]_2X$ with a nitrogen-heterocycle multiatom bridge results in the disappearance of all interactions between the two iron porphyrin units.[8] This is not the case for many non-porphyrin dimeric complexes that are bridged by nitrogen heterocycles. For example, the well-known bridged Ru complexes of the form $[[(NH_3)_5Ru]_2L]^{n+}$, where n = 6, 5 or 4 and L is one of various 4,4′-bipyridyl-type ligands, exhibit extensive interaction between the two metal centers.[9-11] It is thus not clear

(1) Lançon, D.; Kadish, K. M. *Inorg. Chem.* **1984**, *23*, 3942.
(2) Kadish, K. M.; Cheng, J. S.; Cohen, I. A.; Summerville, D. A. In *Electrochemical Studies of Biological Systems*; ACS Symposium Series 38; American Chemical Society: Washington, DC, 1977; Chapter 5.
(3) Kadish, K. M.; Rhodes, R. K.; Bottomley, L. A.; Goff, H. M. *Inorg. Chem.* **1981**, *20*, 3195.
(4) Felton, R. H.; Owen, G. S.; Dolphin, D.; Forman, A.; Borg, D. C.; Fajer, J. *Ann. N.Y. Acad. Sci.* **1973**, *206*, 504.
(5) Chang, D.; Cocolios, P.; Wu, Y. T.; Kadish, K. M. *Inorg. Chem.* **1984**, *23*, 1629.
(6) Bottomley, L. A.; Gorce, J.-N.; Goedken, V. L.; Ercolani, C. *Inorg. Chem.* **1985**, *24*, 3733.
(7) Bottomley, L. A.; Ercolani, C.; Gorce, J.-N.; Pennesi, G. *Inorg. Chem.* **1986**, *25*, 2338.
(8) Gorce, J.-N. Ph.D. Dissertation, Georgia Institute of Technology, 1986.
(9) Creutz, C.; Taube, H. *J. Am. Chem. Soc.* **1969**, *91*, 3988.

0020-1669/88/1327-2320$01.50/0